Full quantum time-dependent simulations for the two-body breakups of H_2Ar^{2+} and N_2Ar^{2+}

Xiaoqing Hu [1,*], Congcong Jia,[1] Ting Xu,[1] Yong Wu,[1,2,†] and Jianguo Wang[1]

[1]*Key Laboratory of Computational Physics, Institute of Applied Physics and Computational Mathematics, Beijing 100088, China*
[2]*HEDPS, Center of Applied Physics and Technology, Peking University, Beijing 10084, China*

We developed a full quantum time-dependent wave-packet evolution method to simulate the multibody breakups of polyatomic molecular ions. The interaction picture theory was used to propagate the wave packet, where the effects of strong and long-range interactions are considered by basis functions and the weak and short-range interactions are included in the perturbation term. In this method, the Coulomb interactions, polycentric interactions, vibration-rotation coupling of molecular fragments, and the rotation-rotation coupling between molecular fragment and parent molecule are considered accurately. Using this method, we simulate the two-body breakups of H_2Ar^{2+} and N_2Ar^{2+}. The simulated results show that the ultrafast rotation of the molecular fragment generally exists in the breakup of the polyatomic molecular ion. For H_2Ar^{2+}, H_2^+ can rotate from an initial broad distribution around $35°$ and $145°$ to a narrow distribution around $75°$ and $105°$ within 30 fs. For N_2Ar^{2+}, the initial sine-shaped angular distribution ($j = 0$) shrinks to a narrow range ($90° \pm 20°$) within 120 fs and then spreads to an approximately random distribution within 300 fs. Such ultrafast rotations are dominated by the polycentric interaction between fragments and impacted by the vibration-rotation and rotation-rotation couplings.

I. INTRODUCTION

One of the most advanced research fields in atomic and molecular physics is the study of polyatomic molecular structure using the Coulomb explosion imaging (CEI) technique. A number of pioneering works have been published in the past decades. A representative work is the reconstruction of CH_4^+ by Vager and coworkers [1], where the CH_4^+ molecule was accelerated to a velocity of approximately 2% of the speed of light and then passed through a thin solid film. As a result, all its valence electrons were removed and the molecule dissociated into several ionic fragments. By measuring the final momentum vectors of all fragments in coincidence, the internuclear distances and bond angles of the projectile could be retrieved. Such technique was also widely extended to ultrafast and strong laser pulses [2], fast electron impact [3], and ion collision [4,5] experiments. Using these techniques, the structures of many molecules were detected correctly, such as CO_2 [5–7], SO_2 [8], N_2Ar [9–11], O_2Ar, O_2Xe [9] and even chiral epoxide [12].

Recently, a Coulomb explosion imaging technique was used to reveal the quantum multibody correlation effect in the multibody breakups of polyatomic molecular ions [13–15]. In 2017, Ding *et al.* investigated the three-body breakup of $(CO)_2^{3+}$ using the laser-based channel-selected CEI [13]. By analyzing the momentum correlation among three fragments, they revealed the ultrafast dissociated mechanism for CO^{2+} in the dimer environment. The result showed that the ultrafast dissociations of CO^{2+} resulted from the symmetry breaking caused by the neighbor ion CO^+, which allowed the rapid

nonadiabatic transition from long-lived metastable state $X^3\Pi$ to the repulsive state $^3\Sigma^-$. More recently, Zhu *et al.* reported an exotic transfer channel involving a heavy N^+ ion observed in a doubly charged cluster produced by 1 MeV Ne^{8+} ions: N_2 - $Ar^{2+} \rightarrow N^+ + NAr^+$ [14]. Another work revealed the ultrafast rotation mechanism of fragment ions in the dimer environment [15].

Compared with the rapid development of experimental technology, the theoretical research on molecular fragmentation dynamics are still at the qualitative or semi-quantitative level [16–18]. For the direct fragmentation dynamics of highly charged molecular ions, the classical point-charge approximation model was mainly used to simulate the fragmentation of molecular ions, where all the fragments were treated as the point charges and only the Coulomb interactions between fragments were considered [19,20]. For the dynamics involving the transition of different electronic states, only the qualitative analysis were provided in theory based on the potential energy curves calculated by the *ab initio* method [21]. Although several semi-classical simulated methods were proposed in the past years [15,22,23], these methods ignored many complex but important interactions, such as the evolution of the vibrational wave packet, vibration-rotation coupling, rotation-rotation coupling, multichannel interference, and the interaction between the laser and molecules. Finally, the lack of a theoretical research ability greatly restricted the understanding of the complex multibody correlation effects involved in the multibody breakups of the molecular ion.

To reveal the micromechanism of multibody breakup dynamics, we developed a full quantum time-dependent wave-packet evolution method. Considering such a Coulomb explosion process dominated by the long-range Coulomb interactions, the interaction picture theory was used to propagate

*Corresponding author: xiaoqing-hu@foxmail.com
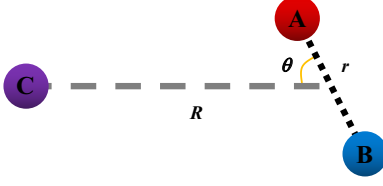†Corresponding author: wu_yong@iapcm.ac.cn

FIG. 1. Schematic diagram of Jacobian coordinates for three-atom system *AB-C*.

the wave packet [24], where the effects of strong and long-range interactions V_0 are considered in the term H_0 and the weak and short-range interactions are included in the perturbation term H'. With this treatment, the simulations of multibody breakups are efficient and accurate.

In this work, we present the theoretical simulations of two-body breakups for H_2Ar^{2+} and N_2Ar^{2+} to test the home-developed time-dependent wave-packet evolution program. These two reactions are appropriate test objectives since the motion in θ are dominated by the very weak polycentric interactions. Such a weak interaction leads to the concerned two-body breakups with very strong quantum properties. Further, the impact of vibration-rotation coupling and rotation-rotation coupling on breakups also can be investigated accurately. The time-dependent rotational energy, rotational quantum number, angular distribution, and total wave packet are given in the present simulations. The results reveal that the ultrafast rotation for molecular fragments are general, even for the breakup of N_2Ar^{2+}, where both the angular stable geometry of neutral N_2Ar and the one of N_2Ar^{2+} are T-shaped.

The organization of this article is as follows. The theoretical framework of the full quantum time-dependent wave-packet evolution method is briefly presented in Sec. II, where essential formulas are derived. In Sec. III, the results are discussed in detail. The conclusion is drawn in Sec. IV. Atomic units are employed throughout the work unless stated otherwise.

II. THEORY

Different from the time-dependent simulation of a neutral particle colliding with an atom, molecule, or ion, the Coulomb explosion of highly charged polyatomic molecule is determined by long-range Coulomb interactions. The strong interaction and complex boundary conditions greatly increase the difficulty of simulation. To reduce the calculation amount of the simulation and ensure the calculation accuracy, the interaction picture theory is used to propagate the wave packet.

A. Hamiltonian of three-atom system

The Hamiltonian of the three-atom system $(AB\text{-}C)^{2+}$ in Jacobi coordinates (as Fig. 1) [25] can be written as

$$H = -\frac{\hbar^2}{2\mu_R}\frac{\partial}{\partial R^2} - \frac{\hbar^2}{2\mu_r}\frac{\partial}{\partial r^2} + \frac{j^2}{2\mu_r r^2} + \frac{(J-j)^2}{2\mu_R R^2} + V(R, r, \theta), \quad (1)$$

where μ_R is the reduced mass of $(AB\text{-}C)^{2+}$ and μ_r is the reduced mass of AB^+. j is the rotational angular momentum

operator of AB^+. J is the total angular momentum operator, which is set as 0 for the breakups of molecules in an ultracold environment. $V(R, r, \theta)$ is defined as the potential energy of the triatomic system and can be partitioned as follows:

$$V(R, r, \theta) = V_{AB^+}(r) + \frac{1}{R} + V'(R, r, \theta), \quad (2)$$

where $V_{AB^+}(r)$ is the potential energy of AB^+, $1/R$ is the Coulomb interaction between AB^+ and C^+, and $V'(R, r, \theta)$ is the residual polycentric interaction. Then, the total Hamiltonian can be written as

$$H = \left[-\frac{\hbar^2}{2\mu_R}\frac{\partial}{\partial R^2} + \frac{1}{R} \right] + \left[-\frac{\hbar^2}{2\mu_r}\frac{\partial}{\partial r^2} + V_{AB^+}(r) \right] + \frac{j^2}{2\mu_r r_0^2}$$

$$+ V'(R, r, \theta) + \frac{j^2}{2\mu_R R^2} + \frac{j^2}{2\mu_r r^2} - \frac{j^2}{2\mu_r r_0^2}$$

$$= H_R + H_r + H_\theta + V'(R, r, \theta) + H'(R, \theta) + H'(r, \theta)$$

$$= H_R + H_r + H_\theta + H' = H_0 + H', \quad (3)$$

where r_0 is the equilibrium position of AB^+. Finally, the Hamiltonians H_R, H_r, and H_θ are independent of the others and their eigenwave functions ψ_R, φ_r, and ϕ_θ are set as the basis functions to describe the nuclear wave function of $(AB\text{-}C)^{2+}$. The perturbation Hamiltonian H' includes the polycentric interaction $V'(R, r, \theta)$, the vibration-rotation coupling term $H'(r, \theta)$, and the rotation-rotation coupling term $H'(R, \theta)$.

B. Time-dependent wave-packet evolution theory

The nuclear wave function of $(AB\text{-}C)^{2+}$ can be written as

$$\Psi(t) = \sum_{lmn} c_{lmn}(t)\psi_l(R)\varphi_m(r)\phi_n(\theta). \quad (4)$$

Based on the interaction picture, the evolution of the nuclear wave function should obey the equation

$$^I\hat{H}\,^I\Psi(t) = i\hbar\frac{\partial}{\partial t}\,^I\Psi(t), \quad (5)$$

where

$$^I\hat{H} = e^{\frac{i}{\hbar}H_0 t}\hat{H}'e^{\frac{-i}{\hbar}H_0 t},$$
$$^I\Psi(t) = e^{\frac{i}{\hbar}H_0 t}\Psi(t). \quad (6)$$

By substituting the $\Psi(t)$ in formula (5) to formula (4) and multiplying it by $\psi_L(R)\varphi_M(r)\phi_N(\theta)$, we can obtain that

$$\dot{c}_{LMN}(t) = \frac{1}{i\hbar}\sum_{lmn} c_{lmn}(t)H'_{LMN,lmn}, \quad (7)$$

where

$$H'_{(LMN,lmb)} = \int \psi_L\varphi_M\phi_N H'\psi_l\varphi_m\phi_n \sin\theta \, dR \, dr \, d\theta. \quad (8)$$

If we expand the coefficient as

$$c_{LMN}(t) = c_{LMN}(t)_0 + c_{LMN}(t)_1 + c_{LMN}(t)_2 + \cdots \quad (9)$$

and assume that

$$c_{LMN}(t)_0 = c_{LMN}(t - dt)e^{-\frac{i}{\hbar}E_{LMN}dt}, \quad (10)$$

then,

$$c_{LMN}(t)_1 = \frac{1}{i\hbar} \sum_{lmn} c_{lmn}(t)_0 H'_{LMN,lmn} dt,$$

$$c_{LMN}(t)_2 = \frac{1}{i\hbar} \sum_{lmn} c_{lmn}(t)_1 H'_{LMN,lmn} dt. \qquad (11)$$

In the present simulation, Eq. (9) only sums to the second order and dt is set as 1.0 a.u. to ensure the convergence of the simulated results.

III. RESULTS AND DISCUSSION

In this work, we simulated the two-body breakups of H_2Ar^{2+} and N_2Ar^{2+} using the full quantum time-dependent wave-packet evolution method. The high-precision CCSD(T) [26] and CASSCF [27,28] methods were used to calculate the potential energy surfaces (PESs) for the neutral dimers and their ions, respectively. Considering the dominant role of the long-range Coulomb potential, the calculated PESs cover a very large area, where R ranges from 5.0 a.u. to 100 a.u., r ranges from 1.5 a.u. to 10.0 a.u., and θ ranges from 0° to 180°. Four thousand, 400, and 1800 grids are used to calculate the independent basis function, ψ_R, φ_r, and ϕ_θ, respectively. The calculated PESs are extended to this three-dimensional grids by least-square's fitting. Then, the initial wave packets are set as the ground vibrational states of neutral dimers and expanded to these three sets of functions. Finally, all the wave-packet evolutions are done in the eigenspace of H_0, which contains 1000 ψ_R, 30 φ_r, and 50 ϕ_θ. It should be noted that the time of the wave-packet evolution must be controlled in a suitable range to avoid the wave packet reaching the boundary, where the wave packet will be bounced due to the infinite potential barrier.

A. Two-body breakup of H_2Ar^{2+}

First, we simulated the two-body breakups of H_2Ar^{2+}. The *ab initio* calculations shown in Fig. 2(a) indicate that the equilibrium geometry of neutral H_2Ar is located at ~8.12 a.u. and 0° and 180° (linear shape). Due to the weak van der Wals bond and the small mass of H_2, the radial distribution center of the ground vibrational state shifts to ~7.34 a.u. The angular vibrational wave funciton is mainly distributed at $j = 1$ with the distribution center at 35° and 145°. Figure 2(c) shows the PES of H_2Ar^{2+} in the ground state. Different from the neutral H_2Ar, the potential energy of H_2Ar^{2+} decreases monotonically from linear shape to T-shaped. Hence, once the ion H_2Ar^{2+} is generated by laser, ion collision, or electron impact, the molecular ion H_2^+ will rotate rapidly. More importantly, it can be seen from Fig. 2(d) that there is an obvious difference between the equilibrium geometry of neutral H_2 and the one of ground H_2^+, which leads to the rapid evolution of the vibrational wave packet of H_2^+ with the increase of R and rotation of θ.

Figure 3 shows the simulated results for the two-body breakup of H_2Ar^{2+}. In total, four models are used in the present simulations, where the $V1$ model only considers the polycentric interaction between H_2^+ and Ar^+, the $V2$ model considers the contributions of the polycentric term

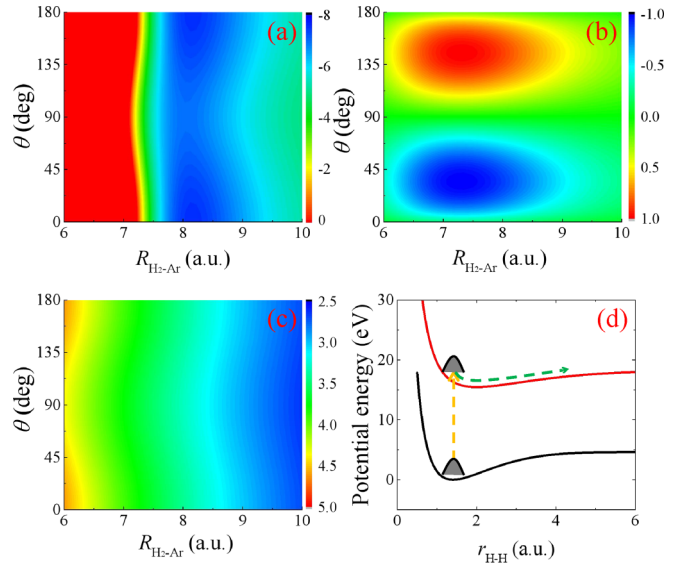FIG. 2. Shown are the used structure information for the two-body breakup of H_2Ar^{2+}. (a) The PES of neutral H_2Ar calculated by CCSD(T), where the distance between two H atoms is set as 1.40 a.u. and energy in meV. (b) The calculated two-dimensional ground vibrational wave function for H_2Ar based on the neutral PES, the integral factor of solid angle $\sin\theta$ was considered in this result. (c) The PES of H_2Ar^{2+} calculated by CASSCF, energy in eV. (d) The potential energy curves(PECs) for H_2^+.

and vibration-rotation coupling term, the $V3$ model considers the contributions of the polycentric term and rotation-rotation coupling term, and the $V4$ model considers all the interactions. Qualitatively, the vibration-rotation coupling [29,30] can
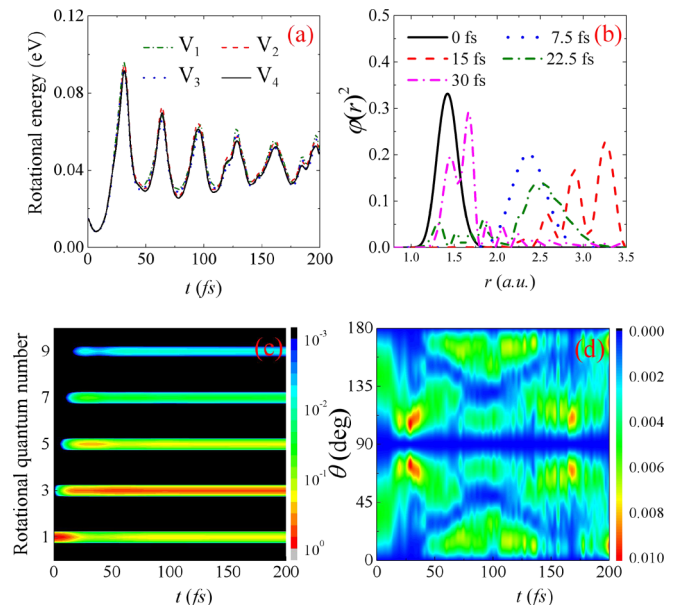

FIG. 3. Shown are the simulated results for the two-body breakup of H_2Ar^{2+}. (a) The time-dependent rotational energy of H_2^+ for four different models. (b) The time-dependent wave packet in r direction for H_2^+. (c) The time-dependent rotational quantum number for H_2^+. (d) The time-dependent angular distribution.
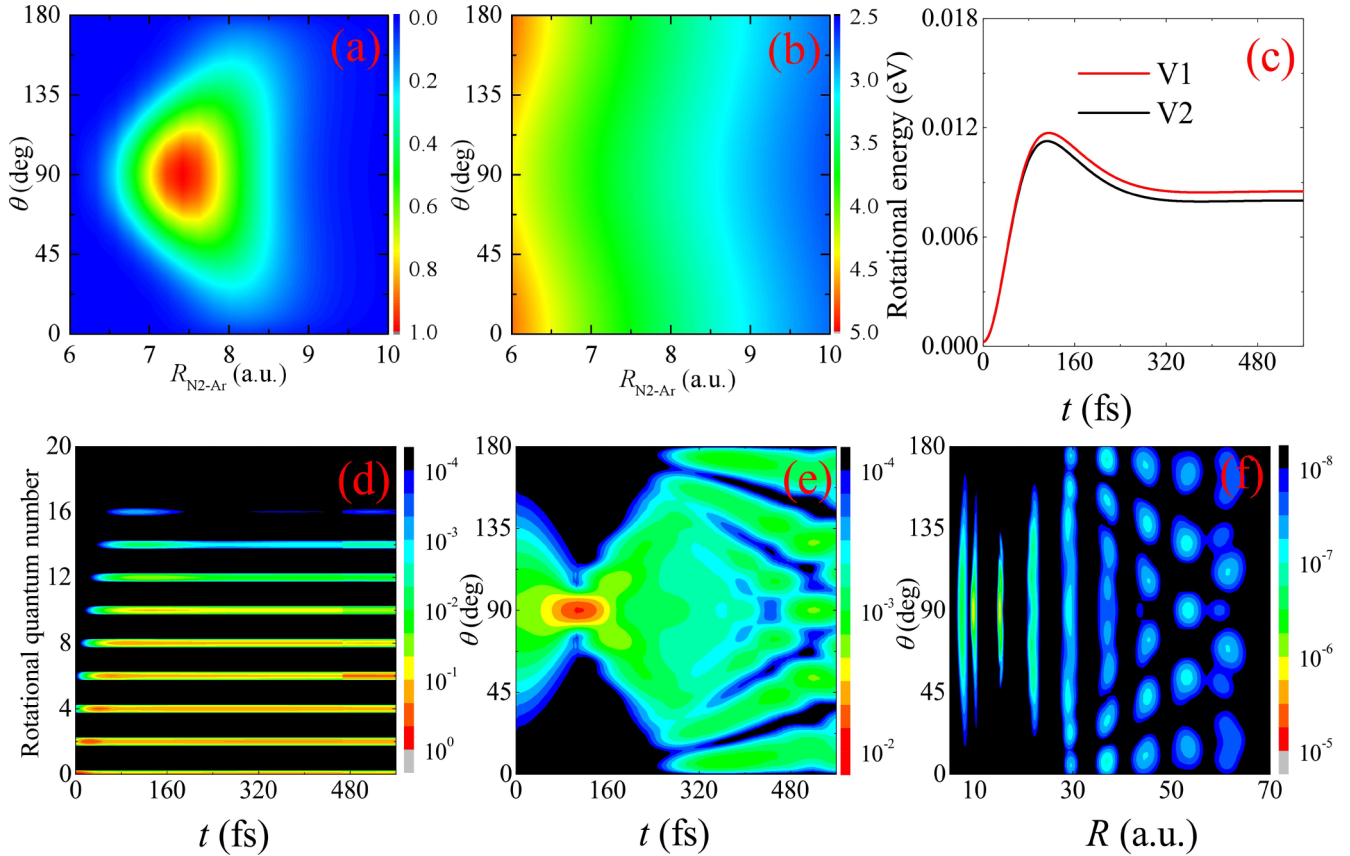
FIG. 4. Shown are the used structural information and simulated results for the two-body breakup of N_2Ar^{2+}. (a) The calculated two-dimensional ground vibrational wave function for N_2Ar based on the neutral PES, the integral factor of solid angle $\sin\theta$ is considered in this result. (b) The PES of N_2Ar^{2+} calculated by CASSCF, energy in eV. (c) The simulated time-dependent rotational energy of N_2^+ for two different models. (d) The time-dependent rotational quantum number for H_2^+. (e) The time-dependent angular distribution. (f) The two-dimensional wave packet for N_2Ar^{2+} with $t = 0, 72, 144, 216, 288, 360, 432, 504$, and 576 fs.

induce the conversion of the vibrational energy and rotational energy of H_2^+, and the rotation-rotation coupling can cause the dimer ion H_2Ar^{2+} to rotate in the opposite direction of H_2^+. Quantitatively, comparing the time-dependent rotational energy spectra calculated by these four models is shown in Fig. 3(a); it is hard to find the obvious differences. The main reason for this is that the vibration-rotation coupling and rotation-rotation coupling in this dissociated process are much weaker than the polycentric interaction between H_2^+ and Ar^+.

Furthermore, the regular oscillation can be found in the time-dependent rotational energy spectra, which is caused by the vibration of H_2^+. The evolution of the vibrational wave packet for H_2^+ is shown in Fig. 3(b), where the bond H-H stretches to ~ 3.0 a.u. at 15.0 fs and then shrinks to 1.6 a.u. at 30 fs. Since the rotational energy is inversely proportional to the square of r, the biggest rotational energy can reach to about 0.095 eV, which is 100 times larger than the free rotation energy. We also simulate the time-dependent rotational quantum number as shown in Fig. 3(c). Due to the antisymmetry of the initial wave packet and the symmetry of the polycentric interaction, the simulated angular wave packet must be antisymmetric and the rotational quantum numbers should remain odd. In this dissociated process, the rotational quantum number can be excited to 9 at ~ 27.0 fs, which corresponds to

a great energy of ~ 0.46 eV. The simulated angular distribution indicates that H_2^+ can rotate from an initial broad distribution around $35°$ and $145°$ to a narrow distribution around $75°$ and $105°$ at ~ 28.8 fs. After a period of evolution, the angular distribution returns to around $70°$ and $110°$ with a narrow distribution at 168.0 fs. The simulated rotational period is about 139.2 fs.

B. Two-body breakup of N_2Ar^{2+}

Using the same method, the two-body breakup of N_2Ar^{2+} is simulated. Different from the H_2Ar^{2+} discussed above, the angular stable geometry of neutral N_2Ar is T-shaped and the one of N_2Ar^{2+} is also T-shaped. For such a system, it is generally believed that the ions do not rotate under the influence of the neighbor. However, our simulations show t completely different results. Only two models are used in the simulations of N_2Ar^{2+}, where the $V1$ model only considers the polycentric interaction and the $V2$ model considers the polycentric interaction and rotation-rotation coupling interaction. The vibration-rotation coupling is neglected since the ground vibrational wave function of N_2^+ is basically the same as the one of neutral N_2 and the vibrational wave packet for the N-N bond does not change in the simulations. In addition, the vibrational excitation is also neglected because the excited energy is much larger than the polycentric interaction.

Figure 4(c) shows the time-dependent rotational energy spectra in these two models. The calculation of the $V1$ model indicates that the polycentric interaction can lead to the rotational excitation for N_2^+. The largest rotational energy can reach about 0.012 eV and finally stabilize at 0.0085 eV. Further, the calculation of the $V2$ model indicates that the rotation-rotation coupling has an obvious influence on the rotational energy. Compared with the calculation for H_2Ar^{2+}, the contribution of rotation-rotation coupling in the breakups of N_2Ar^{2+} is much stronger than it is in H_2Ar^{2+}. Note that the importance of rotation-rotation coupling mainly depends on the ratio between r^2 and R^2. The larger reduced mass of N_2 induces the slower stretching of R and faster rotation for the dimer.

Figure 4(d) shows the time-dependent rotational quantum number. Contrary to the results of H_2Ar^{2+}, the rotational quantum number remains even during the entire dissociated process due to the symmetry sine-shaped initial wave packet ($j = 0$). The simulated results presented in Fig. 4(e) show that the initial sine-shaped angular distribution shrinks to a narrow range ($90° \pm 20°$) within 120 fs and then spreads to an approximately random distribution within 300 fs. The two-dimensional wave packets for N_2Ar^{2+} in Fig. 4(f) also indicate that the angular distribution does not have a clear center, but has many peaks with similar intensity when R is larger than 30.0 a.u. Finally, the orientation of N_2 is close to isotropy. Such results reveal that the change of the shape of PESs will lead to the obvious change of the angular distribution even if the angular stable geometries for neutral molecules and its ions are consistent.

IV. SUMMARY AND CONCLUSION

In this paper, a home-developed full quantum time-dependent wave-packet evolution method was presented to simulate the multibody breakups of polyatomic molecular ions. Using this method, we simulated the two-body breakups of H_2Ar^{2+} and N_2Ar^{2+} and investigated the ultrafast rotation of molecular fragments in the dimer environment. The result indicates that the polycentric interaction between molecular ion and its neighbor not only induces the ultrafast rotation of the molecular fragment for the dimer with different angular stable geometries in neutral and charged states, but also significantly affects the angular distribution of the molecular fragment for those systems, where the initial angular stable geometries are the same as the ones of charged ions. Based on this investigation, we conclude that the rotation caused by the neighbor ion exists in all the fragmentation of polyatomic molecular ions.

More importantly, since the used three sets of independent basis functions are the eigen-wave-functions of H_0, which includes all the kinetic energy terms and the major potential energy terms, the corresponding eigenenergies, vibrational, and rotational quantum numbers are physical and can reflect the real breakup dynamics. Furthermore, these dynamic information also can help us improve the efficiency of simulations by reducing the number of basis functions needed in the expansion of the wave packet. For example, for the dynamics with excitation caused by radial coupling, the basis sets of the excited state only need to include those bases with the close energy as the intersection point. Similarly, for the dynamics with excitation by absorbing photons, the energy conservation law can also be used to narrow the expansion range of the basis set. Therefore, this method would be appropriate and efficient to study more complex fragmentation dynamics involving multichannel transition and external field.

[1] Z. Vager, R. Maaman, and E. P. Kanter, Science **244**, 426 (1989).

[2] T. Weber, A. O. Czasch, O. Jagutzki, A. K. Müller, V. Mergel, A. Kheifets, E. Rotenberg, G. Meigs, M. H. Prior, S. Daveau *et al.*, Nature (London) **431**, 437 (2004).

[3] X. Ren, E. Wang, A. D. Skitnevskaya, A. B. Trofimov, K. Gokhberg, and A. Dorn, Nat. Phys. **14**, 1062 (2018).

[4] A. Mery, A. N. Agnihotri, J. Douady, X. Flechard, B. Gervais, S. Guillous, W. Iskandar, E. Jacquet, J. Matsumoto, J. Rangama, F. Ropars, C. P. Safvan, H. Shiromaru, D. Zanuttini, and A. Cassimi, Phys. Rev. Lett. **118**, 233402 (2017).

[5] N. Neumann, D. Hant, L. Ph. H. Schmidt, J. Titze, T. Jahnke, A. Czasch, M. S. Schöffler, K. Kreidi, O. Jagutzki, H. Schmidt-Böcking, and R. Dörner, Phys. Rev. Lett. **104**, 103201 (2010).

[6] I. Bocharova, R. Karimi, E. F. Penka, J. P. Brichta, P. Lassonde, X. Fu, J. C. Kieffer, A. D. Bandrauk, I. Litvinyuk, J. Sanderson, and F. Légaré, Phys. Rev. Lett. **107**, 063201 (2011).

[7] C. Wu, C. Wu, D. Song, H. Su, Y. Yang, Z. Wu, X. Liu, H. Liu, M. Li, Y. Deng, Y. Liu, L. Y. Peng, H. Jiang, and Q. Gong, Phys. Rev. Lett. **110**, 103601 (2013).

[8] F. Légaré, Kevin F. Lee, I. V. Litvinyuk, P. W. Dooley, A. D. Bandrauk, D. M. Villeneuve, and P. B. Corkum, Phys. Rev. A **72**, 052717 (2005).

[9] J. Wu, M. Kunitski, L. Ph. H. Schmidt, T. Jahnke, and R. Dörner, J. Chem. Phys. **137**, 104308 (2012).

[10] C. Wu, C. Wu, D. Song, H. Su, X. Xie, M. Li, Y. Deng, Y. Liu, and Q. Gong, J. Chem. Phys. **140**, 141101 (2014).

[11] J. Wu, X. Gong, M. Kunitski, F. K. Amankona-Diawuo, L. Ph. H. Schmidt, T. Jahnke, A. Czasch, T. Seideman, and R. Dörner, Phys. Rev. Lett. **111**, 083003 (2013).

[12] P. Herwig, K. Zawatzky, M. Grieser, O. Heber, B. Jordon-Thaden, C. Krantz, O. Novotný, R. Repnow, V. Schurig, D. Schwalm *et al.*, Science **342**, 1084 (2013);

[13] X. Ding, M. Haertelt, S. Schlauderer, M. S. Schuurman, A. Yu. Naumov, D. M. Villeneuve, A. R. W. McKellar, P. B. Corkum, and A. Staudte, Phys. Rev. Lett. **118**, 153001 (2017).

[14] X. L. Zhu, X. Q. Hu, S. C. Yan, Y. G. Peng, W. T. Feng, D. L. Guo, Y. Gao, S. F. Zhang, A. Cassimi, J. W. Xu, Do. M. Zhao, D. P. Dong, B. Hai, Y. Wu, J. G. Wang, and X. Ma. Nat. Commun. **11**, 2987 (2020)

[15] X. Q. Hu, Y. G. Peng, X. L. Zhu, S. C. Yan, L. Liu, W. T. Feng, D. L. Guo, Y. Gao, S. F. Zhang, D. M. Zhao, D. P. Dong, B. Hai, J. W. Xu, S. B. Zhang, X. Ma, J. G. Wang, and Y. Wu, Phys. Rev. A **101**, 012707 (2020)

[16] X. Gong, M. Kunitski, L. Ph. H. Schmidt, T. Jahnke, A. Czasch, R. Dörner, and J. Wu, Phys. Rev. A **88**, 013422 (2013).

[17] C. Wu, Y. Yang, Z. Wu, B. Chen, H. Dong, X. Liu, Y. Deng, H. Liu, Y. Liu, and Q. Gong, Phys. Chem. Chem. Phys. **13**, 18398 (2011).

[18] I. A. Bocharova, A. S. Alnaser, U. Thumm, T. Niederhausen, D. Ray, C. L. Cocke, and I. V. Litvinyuk, Phys. Rev. A **83**, 013417 (2011).

[19] K. Kwon and A. Moscowitz, Phys. Rev. Lett. **77**, 1238 (1996).

[20] B. Ulrich, A. Vredenborg, A. Malakzadeh, L. Ph. H. Schmidt, T. Havermeier, M. Meckel, K. Cole, M. Smolarski, Z. Chang, T. Jahnke, and R. Dörner, J. Phys. Chem. A **115**, 6936 (2011).

[21] C. Küstner-Wetekam, X. Q. Hu, L. Marder, Ph. Schmidt, C. Ozga, Ch. Zindel, H. Otto, Y. G. Peng, J. G. Wang, C. Richter, N. Sisourat, U. Hergenhahn, A. Knie, A. Ehresmann, Y. Wu, and A. Hans, Phys. Rev. A **104**, 042802 (2021).

[22] H. J. Yang, E. Wang, W. X. Dong, M. Gong, Z. Shen, Y. Tang, X. Shan, and X. Chen, Phys. Rev. A **97**, 052703 (2018).

[23] H. Yang, M. Gong, W. Dong, and Z. Shen, E. Wang, and X. Chen., J. Phys. B: At. Mol. Opt. Phys. **51**, 245201 (2018).

[24] C. J. Williams, J. Qian, and D. J. Tannor, J. Chem. Phys. **95**, 1721 (1991).

[25] P. Zhang and K. Han, J. Phys. Chem. A **118**, 8929 (2014).

[26] H.-J. Werner, P. J. Knowles, G. Knizia, F. R. Manby, M. Schütz, P. Celani, T. Korona, R. Lindh, A. Mitrushenkov, G. Rauhut *et al.*, MOLPRO, a package of *ab initio* programs, version 2010.1 (2010). See http://www.molpro.net.

[27] P. J. Knowles and H.-J. Werner, Chem. Phys. Lett. **115**, 259 (1985).

[28] H. J. Werner, P. J. Knowles, G. Knizia, F. R. Manby, and M. Schütz, WIREs Comput Mol Sci **2**, 242 (2012).

[29] V. Laporta, J. Tennyson, and R. Celiberto, Plasma Sources Sci. Technol. **25**, 06LT02 (2016).

[30] V. Laporta, K. Chakrabarti, R. Celiberto, R. K. Janev, J. Z. Mezei, S. Niyonzima, J. Tennyson, and I. F. Schneider, Plasma Phys. Control. Fusion **59**, 045008 (2017).